Scalable Computing: Practice and Experience, ISSN 1895-1767, http://www.scpe.org
© 2024 SCPE. Volume 25, Issues 3, pp. 1387–1401, DOI 10.12694/scpe.v25i3.2691

CLASSIFICATION OF COVID-19 USING DIFFERENTIAL EVOLUTION CHAOTIC WHALE OPTIMIZATION BASED CONVOLUTIONAL NEURAL NETWORK

D.P. MANOJ KUMAR*, SUJATA N PATIL†, PARAMESHACHARI BIDARE DIVAKARACHARI ‡, PRZEMYSŁAW FALKOWSKI-GILSKI§, AND R. SUGANTHI¶

Abstract. COVID-19, also known as the Coronavirus disease-2019, is an transferrable disease that spreads rapidly, affecting countless individuals and leading to fatalities in this worldwide pandemic. The precise and swift detection of COVID-19 plays a crucial role in managing the pandemic's dissemination. Additionally, it is necessary to recognize COVID-19 quickly and accurately by investigating chest x-ray images. This paper proposed a Differential Evolution Chaotic Whale Optimization Algorithm (DECWOA) based Convolutional Neural Network (CNN) method for identifying and classifying COVID-19 chest X-ray images. The DECWOA based CNN model improves the accuracy and convergence speed of the algorithm. This method is evaluated by Chest X-Ray (CXR) dataset and attains better results in terms of accuracy, precision, sensitivity, specificity, and F1-score values of about 99.89%, 99.83%, 99.81%, 98.92%, and 99.26% correspondingly. The result shows that the proposed DECWOA based CNN model provides accurate and quick identification and classification of COVID-19 compared to existing techniques like ResNet50, VGG-19, and Multi-Model Fusion of Deep Transfer Learning (MMF-DTL) models.

Key words: Chest X-ray Images, Convolutional Neural Network, COVID-19, Inertia Weight, Residual Blocks.

1. Introduction. The Transfer Learning (TL) is a popular method for developing deep learning models. In the TL, the neural networks are trained in double phases, such as pretraining and fine-tuning [1]. In the first phase, the network is trained commonly on the huge-scale standard dataset which presents an extensive variety of classes [2]. In the next stage, the pretrained network is again trained on the precise target which contains some branded samples than the pretrained dataset [3]. This pretrained stage is useful for the network to learn common features which are to be reprocessed on the target task [4]. These two categories are enormously widespread in numerous situations specifically in therapeutic images. In TL, the benchmark structures are considered for ImageNet with matching pre-trained weights that are fine-tuned on clinical tasks extending from the COVID-19 diagnosis [5]. COVID-19 is considered by huge transmittable disease and death rate. Every country has employed various productive measures to the safety of their citizens [6].

The major promising study parts in the healthcare domain and the technical group are concentrated on medical applications like creating of Computer-Aided Diagnosis (CAD) system for chest X-ray images [7]. By utilizing transfer learning, healthcare experts can influence the knowledge and proficiency within these pre-trained models and apply it to several healthcare tasks such as disease diagnosis, prediction, and medical image analysis [8]. This technique saves time and improves the accuracy and efficiency of healthcare systems [9]. COVID-19 is a transportable disease produced by the SARS-CoV-2 virus. It rapidly circulates and a wide variety of people endure and die from this unive rsal pandemic [10]. Coronavirus is a large family virus and SARS-CoV-2 is a ribonucleic acid (RNA) virus which comes under coronaviruses [11]. COVID-19 is identified over various approaches such as chest X-ray, positive pathogenic test, CT images, epidemiological history and medical syndromes such as pneumonia, cough, dyspnea and fever [12]. The utilization of chest X-ray and CT scans is beneficial in the premature treatment and diagnosis of the disease. The advantage of using these CT

*Department of Computer Science and Engineering, Kalpataru Institute of technology, Tiptur -572201, India
†Radiation Oncology Department (Pathology lab), Thomas Jefferson University Philadelphia, PA, 19107, USA
‡Department of Electronics and Communication Engineering, Nitte Meenakshi Institute of Technology, Bengaluru 560064, Visvesvaraya Technological University, Belagavi, India. (paramesh@nmit.ac.in).
§Faculty of Electronics, Telecommunications and Informatics, Gdansk University of Technology, Narutowicza 11/12, 80-233 Gdansk, Poland
¶Department of Electronics and Communication Engineering, Panimalar Engineering College, Chennai, India

and Chest X-rays is high speed, cost-effectiveness, and a wide range of applications [13]. The detection of COVID-19 in X-ray images is a difficult task because of the requirements of trademark and the accuracy is amplified by the process of segmentation. In recent times, methods based on deep learning has majorly utilized in medical image classification. There is a chance for acquiring much noises while obtaining the X-ray images. So, the technique of noise removal is important for decreasing the noise. The selection of features plays a major role in the part of classification, because it decreases the evaluation time and maximizes the performance of classification. The application of deep learning produces an ideal solution because it extracts many prominent features from whole image than the manually defined features. In the pandemic situation, the critical problem of COVID-19 is the distribution of rapid treatment to the patients. Due to the rapid spread of pandemic, the patients are severely admitted to the hospitals which leads the requirement of faster diagnosis models need to be solved.The major contribution of this manuscript is as follows:

- The preprocessing is done by using the which removes the noise from chest X-ray images and feeds into the Multilevel threshold segmentation process which enhances the training process and minimizes the overfitting issues.
- After the segmentation, the segmented chest X-ray image features are extracted by shape, texture, color and ResNet50 then selected by using DECWOA, and these features are given as input to the CNN classifier.
- By integrating the chaotic nature of WOA enhances the exploration of the solution space which is utilized to find optimal solutions in the high dimensional and complex space. The DECWOA helps in tuning the parameters of CNN to adopt the complex data patterns and enhancing the model performance.

The rest part of research is as follows: Section 2 defines literature review. Section 3 defines details of proposed methodology. Section 4 defines results and discussion and Section 5 defines conclusion and lastly this paper finish with the references.

2. Literature Review. Amin Ul Haq et al. [14] introduced a deep learning (DL) and transfer learning (TL) technique for accurate diagnosis of COVID-19 by employing X-ray images of medical information in healthcare. The developed model utilized a 2D Convolutional Neural Network (2DCNN) to enhance the training process. The TL was pretrained by using ResNet-50 which was transferred to 2DCNN model and fine-tuned through X-ray image. Additionally, data augmentation was employed for the training of the (ResNet-50+2DCNN) multiclassification (R2DCNNMC) model. The developed model utilizes computer vision tasks for effectively classifying the images. However, this model is not suitable for all scenarios due to its computational complexity and data requirements.

Rohit Kundu et al. [15] developed an ensemble of three various transfer learning methods for predicting COVID-19 infection through chest CT images. The bagging or bootstrap aggregation of three example models such as Inception v3, ResNet34 and DenseNet201 are utilized to boost the individual model performance. The developed ET-NET method was estimated on publicly available datasets by using 5-fold cross-validation. The developed model required minimum time for attaining the test output and it has minimum FNR. The developed model is incapable of detecting the current COVID-19 infections from the initial infection stage.

Md. Belal Hossain et al. [16] implemented a TL with fine-tuned ResNet50 to classify COVID-19 from chest images. The developed model was altered by attaching a dual fully connected layer to the actual ResNet50 method by employing fine-tuning. The experiments are conducted on COVID-19 Radiography dataset by applying ten various pre-trained weights trained on large-scale datasets. The developed model obtains better accuracy in classifying normal and COVID patients on chest X-ray images. The developed model accomplished transfer learning on limited clinical image datasets and computing resources.

Soarov Chakraborty et al. [17] introduced a transfer learning approach for classifying pneumonia and COVID-19-affected chest X-ray images by utilizing deep CNN on pre-trained VGG-19 architecture. This developed model utilized a MongoDB database for storing original images and respective classes. The developed model performance was measured for classification of COVID-19, pneumonia-affected, and healthy people from chest images. By utilizing a pre-trained model, it achieves better accuracy. However, MongoDB cannot retain a document file which crosses 16MB in size.

A. Siva Krishna Reddy et al. [18] developed a Multi-Model Fusion of Deep Transfer Learning (MMF-DTL)

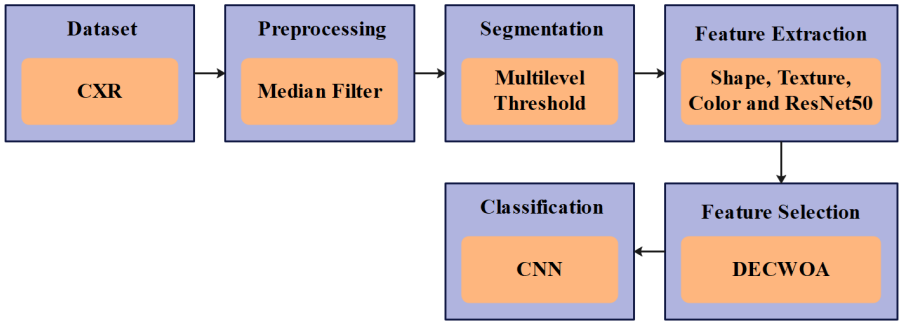

Fig. 3.1: Block Diagram of the Proposed Methodology

approach for the diagnosis and categorization of COVID-19 chest images. The developed model utilized three various DL methods such as Inception v3, VGG16, and ResNet50 for feature selection. The solitary modality was not suitable to obtain an efficient detection rate, the combination of three techniques utilized an MMF to enhance the detection value. At last, the softmax classifier utilized sample images to group six variants. The developed model is utilized to reduce the diagnosis procedure and manage the current epidemic. Hence the developed model cannot be experienced on actual-time images.

Placido L. Vidal et al. [19] suggested a multiple-phase transfer learning for lung segmentation employing transportable X-ray images to COVID-19 patients. The developed model adopts the knowledge from well-known field with numerous samples to a new field with minimized numbers and better complexity. Transfer learning of multiple stages among created consecutive image fields works with a restricted quantity of transportable X-ray models. The advantage of using this model was to train with a huge number of images from the same image field. The limitation of the developed method was established in the images as a minor loss in accuracy and softness in marginal segmentation areas that depend on the image rescaling.

Md. Milon Islam et al. [20] presented a transfer learning based combined Convolutional Neural Network and Recurrent Neural Network (CNN-RNN) technique for COVID-19 diagnosis. The VGG19, InceptionV3, ResNetV2, and DenseNet121 are utilized in this experiment where the CNN was applied to extract the difficult features from samples and RNN was applied to classify them. At last, the images were visualized in the decision-making region by using gradient-weighted class activation mapping. The developed model works only with anterior-posterior view in chest X-ray so, it is unable to classify other views like lordotic, apical, etc.

N. Kumar et al. [21] implemented a deep transfer learning method for detecting COVID-19 patients by utilizing chest X-ray images. The developed method combined several transfer learning methods like Xception-Net, GoogLeNet, and EfficientNet. This model can classify the patient as infected with pneumonia, COVID-19, tuberculosis, or healthy. The developed model employed pre-trained models to extract the features and classify them by utilizing pre-trained models. This model enhances the ability of a classifier for both COVID-19 binary and multiclass datasets. The developed model achieves better diagnosis results with a reduction in errors. However, this model maximizes the training and testing time.

3. Proposed Method. The chest X-ray (CXR) dataset is utilized in this paper which includes 305 images with six different classes. The preprocessing utilizes the median filter which removes the noise from CXR images. The preprocessed data are segmented by using the multilevel threshold image segmentation method. Multilevel thresholding is utilized to choose the attribute to split the image grayscale into more than twofold sets. After segmentation, the features are extracted using shape, texture, color and ResNet50-based feature extraction. The DECWOA is used for selecting the features. The selected features are classified by using Convolutional Neural Network (CNN). The block diagram of the proposed methodology is presented in Figure 3.1.

3.1. Dataset. The dataset used in this analysis is Chest X-Ray (CXR) dataset [22] which is publicly available on the Kaggle. This dataset includes 305 images with six different classes ARDS, COVID-19, No findings, Pneumocystis, SARS, and Streptococcus. The size of every input image is 256×256. These classes

Table 2.1: Key characteristics of previous studies and the proposed solutions

Author	Advantage	Limitation
Amin Ul Haq et al. [14]	The ResNet-50+2DCNN model utilizes computer vision tasks for effectively classifying the images.	However, this model is not suitable for all scenarios due to its computational complexity and data requirements.
Rohit Kundu et al. [15]	The ET-NET model required minimum time for attaining the test output and it has minimum FNR.	The developed model is incapable of detecting the current COVID-19 infections from the initial infection stage.
Md. Belal Hossain et al. [16]	The ResNet50 model obtains better accuracy in classifying normal and COVID patients on chest X-ray images.	The developed model accomplished transfer learning on limited clinical image datasets and computing resources.
Soarov Chakraborty et al. [17]	The VGG-19 model performance was measured for the classification of COVID-19, pneumonia-affected, and healthy people from chest images. By utilizing a pre-trained model, it achieves better accuracy.	However, MongoDB cannot retain a document file that crosses 16MB in size.
A. Siva Krishna Reddy et al. [18]	The MMF-DTL model is utilized to reduce the diagnosis procedure and manage the current epidemic.	Hence the developed model cannot be experienced on actual-time images.
Placido L. Vidal et al. [19]	The U-Net CNN model was utilized to train with a huge number of images from the same image field.	The limitation of the developed method was established in the images as a minor loss in accuracy and softness in marginal segmentation areas that depend on the image rescaling.
Md. Milon Islam et al. [20]	The VGG19-RNN achieves better diagnosis results with a reduction in errors.	The developed model works only with anterior-posterior view in chest X-ray so, it is unable to classify other views like lordotic, apical, etc.
N. Kumar et al. [21]	The ensemble model enhances the ability of a classifier for both COVID-19 binary and multiclass datasets.	However, this model maximizes the training and testing time.
Proposed methodology	By integrating the chaotic nature of WOA enhances the exploration of the solution space which is utilized to find optimal solutions in the high dimensional and complex space. The DECWOA helps in tuning the parameters of CNN to adopt the complex data patterns and enhancing the model performance.	

Table 3.1: Description of CXR Dataset

Classes	ARDS	COVID-19	No findings	Pneumocystis	SARS	Streptococcus
Labels	0	1	2	3	4	5
No of Images	15	220	27	15	11	17

along with corresponding labels and number of images are represented in Table 3.1.The Figure 3.2 presents the sample dataset images.

3.2. Preprocessing. The median filter is a process of nonlinear method which removes the noise [23] from chest X-ray images. Median filter process by shifting pixel in image, modifying every value with median value of adjacent pixel. The pixel is measured by dividing whole values of pixel from neighborhood pattern into the mathematical order and modifying pixel which is considered as average value of pixel. Median filter removes

Fig. 3.2: Sample dataset image

the noise effectively without minimizing the image sharpness which is represented in Eq. 3.1,

$$f(x,y) = median\{g(s,t)\}, where(s,t) \in S_{xy} \tag{3.1}$$

where, S_{xy} represents a group of coordinates in rectangular image window that contains center at (x,y). The $f(x,y)$ is a restored image, $g(s,t)$ is a calculated and corrupted area under S_{xy}.

3.3. Segmentation. The preprocessed data are segmented by using multilevel threshold image segmentation method. Applying multiple thresholds enables the enhancement of contrast a visibility of different structures within the chest X-ray. The thresholding is utilized to choose the attribute to split the image grayscale into more than double sets. It is generally established based on histograms produced by gray-level images. The image is unable to be distributed by noise and histogram of a segmented image has more than two peaks during an ideal condition. Then the threshold is set at trough and'an image is divided into numerous objects and backgrounds. The image is distributed in various noises in an actual picture and image grayscale data is not accurate. There is no peak on the histogram then it is distributed by using noise. The result of image segmentation with a threshold on troughs is incorrect or deprived. In this paper, Kapur's entropy MIS is utilized by non-local means 2D-histogram. When an image is polluted by noise, this technology efficiently minimizes the noise interface and it has a better segmentation effect. The particular procedure is to achieve grayscale image according to an actual image and accomplish a non-local mean noise decrease process on a gray scale image and attained image is known as NLM image. Next, the 2D -histogram is attained corresponding NLM and grayscale images. The highest Kapur's entropy evaluation is performed based on a 2D-histogram then the threshold set according to the highest entropy at last image segmentation is performed with corresponding thresholds. The three-majority image segmentation calculation approaches utilized in this paper which is illustrated in the following section.

3.3.1. Kapur's Entropy. Kapur's entropy is according to the image gray scale which is stored in 8 bits and the range of gray value 0 to 255 . Consider L = 256, n_i is the pixel number grayscale is i. Kapur's entropy H is represented by using Eq. 3.2, Eq. 3.3 and Eq. 3.4.

$$N = \sum_{i=0}^{L-1} n_i \tag{3.2}$$

$$p_i = \frac{n_i}{N} \tag{3.3}$$

$$H = -\sum_{i=0}^{L-1} p_i \ln p_i \tag{3.4}$$

where p_i is incidence of gray scale probability i. For Multilevel threshold Image Segmentation (MIS), images are separated into m subclasses. Where, the $C_0 = \{1, 2, \ldots, t_1 - 1\}, C_1 = \{t_1, \ldots t_2 - 1\}, C_2 = \{t_2, \ldots t_3 - 1\}, \ldots,$ $C_{m-1} = \{t_{m-1}, \ldots L - 1\}$ then the Kapur's entropy H_c is represented by using Eq. 3.5, Eq. 3.6, Eq. 3.7 and Eq. 3.8,

$$H_C = \sum_{i=0}^{m-1} H_{C_i} \tag{3.5}$$

$$H_{C_i} = -\sum_{j=t_i}^{t_{i+1}-1} \frac{p_j}{\omega_i} \ln \frac{p_j}{\omega_i} \tag{3.6}$$

$$\omega_i = \sum_{n=t_i}^{t_{i+1}-1} p_j \tag{3.7}$$

$$t^* = \text{argMax}\,(H_c) \tag{3.8}$$

where the t^* separates the point set when H_c take the highest value which is determined by the threshold.

3.3.2. Non-local means 2D histogram. The non-local means 2D histogram procedure is utilized for maintaining and denoising the highest features of an image. Consider the original image is O, denoising image is N, grayscale of pixel p in image O is represented as $O(p)$. The non-local mean filtering a gray scale $N(p)$ of pixel p is attained by the Eq. 3.9, Eq. 3.10, Eq. 3.11 and Eq. 3.12,

$$N(p) = \frac{\sum_{q \varepsilon O} O(q)\omega(p,q)}{\sum_{q \varepsilon O} \omega(p,q)} \tag{3.9}$$

$$\omega(q,p) = \exp^{-\frac{|\mu(p)-\mu(q)|^2}{\partial^2}} \tag{3.10}$$

$$\mu(p) = \frac{\sum_{i \varepsilon O(p)} O(i)}{m \times m} \tag{3.11}$$

$$\mu(q) = \frac{\sum_{i \varepsilon O(q)} O(i)}{m \times m} \tag{3.12}$$

where, $\omega(q,p)$ is the pixel p and q weights, $L(p)$ and $L(q)$ is the local and centered image on pixel p and q respectively, $\mu(p)$ and $\mu(q)$ are local mean of pixels p and q and ∂ is the standard deviation. By combining the grayscale image O and denoising image N, the 2D view of the histogram is generated and non-local means 2D-histogram is formulated as Eq. 3.13,

$$P_{ij} = \frac{h_{ij}}{m \times n} \tag{3.13}$$

where i and j denotes the pixel rate of image $O(x,y)$ and $N(x,y), h_{ij}$ represents the number of times occurs at gray scale vector (s,t), the pixel size in the image is $m \times n$.

3.3.3. Kapur's entropy-based 2D histogram. The transverse of 2D histogram includes suitable image data. The optimal solution found by $\{t, t_2 \dots t_n - 1\}$ is the optimal threshold. This manuscript estimates Kapur's entropy as an objective function and subareas of major diagonal by utilizing Eq. 3.14,

$$H(s,t) = -\sum_{i=0}^{s_1}\sum_{j=0}^{t_1}\frac{P_{ij}}{P_1}\ln\frac{P_{ij}}{P_1} - \sum_{i=s_1+1}^{s_2}\sum_{j=t_1+1}^{t_2}\frac{P_{ij}}{P_2}\ln\frac{P_{ij}}{P_2}\dots - \sum_{i=s_{L-2}+1}^{s_{L-1}}\sum_{j=t_{L-2}+1}^{t_{L-1}}\frac{P_{ij}}{P_{L-1}}\ln\frac{P_{ij}}{P_{L-1}} \tag{3.14}$$

3.4. Feature Extraction. After the segmentation process, features are extracted using shape, texture, color and ResNet50-based feature extraction. By using this technique, the CXR dataset is much more informative. The shape captures geometric properties, texture accounts for surface patterns, color represents visual information and RsNet50 captures deep learning features.

3.4.1. Shape-based Feature Extraction. The shape-based feature extraction is primarily performed to the shape properties like region, moment, and boundary in the image. Such extraction simplifies the transmission, identification, recognition, and comparison of the shape. Shape-based features must be robust to conversion, scaling, and rotation. In this concern, there is no arithmetical transformation is implicated in shape features. The image has three values in every pixel and in the shape feature extraction the color image is converted into the greyscale images. For this purpose, the Eq. 3.15 is introduced by Craig as shown below:

$$I_g = [I_r I_g I_b] \times 0.29890.5870.114 \tag{3.15}$$

where I_g is the grey-level image, $I_r I_g I_b$ is the component of the color. Neurotrophic clustering is used to divide pixels with the nearest value and avoid pixels from greyscale images.

3.4.2. Texture-based Feature Extraction. The texture-based feature extraction is based on extracting several features from a Grey Level Co-occurrence Matrix (GLCM) model. This GLCM is an effective and robust methodology that analyzes images and it is represented as a combined 2D matrix between pixels and pairs with distance d and the direction θ. To classify the texture features, 14 features such as contrast, correlation, energy, homogeneity, angular second moment, sum of squares variance, inverse different moment, sum average, sum variance, sum entropy, entropy, difference variance, difference entropy and information measure of correlation are extracted from the GLCM method. The texture-based feature extraction using GLCM is presented in the following steps:

- The colored image is converted into a greyscale image.
- Input image is filtered by using 5×5 matrix of Gaussian filter.
- The filtered image is separated into 4×4 matrix blocks.
- The GLCM evaluates every block of energy, contrast, mean value, standard deviation, and homogeneity. The evaluation is done with four directions of these features namely vertical, horizontal, and diagonal direction.
- These extracted features are stored in a database.

3.4.3. Color-based Feature Extraction. The color space demonstrates the color with the appearance of intensity value, it can visualize, specify and create the color through the color space technique. There are three various techniques in color-based feature extraction. The first is the histogram intersection (HI) method which examines global color features. In the HI method, the number of bins creates effects on the performance. The huge number of bins shows the image is difficult and it enhances the computational complexity. The second is Zernike Chromaticity Distribution moments which is derivative from chromaticity space. This model provides accurate length and efficient computation presentation of an image that includes the color of the image but the size differs under flipping and rotation. The third is color histogram that illustrates the image from various perceptions. In this, the regularly distributed color bin is presented and it counts the pixels that are the same and keeps it.

3.4.4. ResNet50-based Feature Extraction. The ResNet utilized the residual block for solving gradient vanishing and degradation problems that happen in CNN model. The residual block increases network potency and performance. It is proficient of generating best output in classifications. The residual block of this

model implements residual below an inclusion of current residual block and replication overcome of the residual block. The residual function is presented in Eq. 3.16,

$$y = F(x, W) + x \tag{3.16}$$

where x, y, and W denote the input, output, and weight of the residual block. It contains various residual blocks in which a kernel size of convolution layer has differed. After feature extraction, the extracted features are selected by the DECWOA model.

3.5. Feature Selection. After extracting features, the DECWOA is used for feature selection. The DECWOA is utilized to overcome the limitations of the WOA [24] like low convergence speed, insufficient ability of global optimization, and easy fall into local optimization. In DECWOA, initial population is produced through presenting Sine Chaos theory at start of an algorithm for improving popularity diversity. Then, new adaptive inertia weight is familiarized into whale individual position update equation to untrained global search and enhancing the performance of optimization. At last, a Differential Evolution algorithm DEA is presented to improve WOA accuracy and global search speed.

3.5.1. Sine Mapping Population Initialization. The population initialization technique affects the accuracy and convergence speed of a particular algorithm. The WOA is utilized as initial random populations in the nonappearance of appropriate experimental data which results in incapability to confirm that whales are regularly circulated through the solution space. Chaotic mapping produces sequences randomly from inevitable schemes that are stochastic and ergodic. 1D chaotic mapping like sine mapping and logistic mapping has a simple structure and high computational speed. Thus, sine chaos is utilized for population initialization of WOA. The sine chaos self-mapping is formulated in Eq. 3.17,

$$x_{n+1} = \sin\left(\frac{2}{x_n}\right), \quad x = 0, 1, \ldots, N \tag{3.17}$$

where x_n represents primary value which cannot be 0 , by evading zero point and immobility range of $[-1, 1]$. At the iteration, the scheme results traverse every solution space.

3.5.2. Adaptive Inertia Weights. The inertia weight parameter is significant in WOA and a persistent inertia weight minimizes an algorithm's effectiveness which cannot behelpful for global optimization algorithms. The maximum inertia weights are helpful for global optimum and minimum inertia weights are helpful for local mining. The ideal inertia weight contains some features: At initial iteration, it has maximum weights which ensures the algorithm has a robust global search ability. At the final iteration, it has minimum weights which ensures the algorithm has a robust local search ability. Thus, the inertia weight helps balance the local and global exploitation capability. The adaptive inertia weight ω is presented in Eq. 3.18,

$$\omega = 0.5 + \exp\left(\frac{-f_{\text{fit}}\,(x)}{u}\right)^{t} \tag{3.18}$$

where, $f_{fit}(t)$ is the whale x fitness value, t is the present number of iterations and u is the greatest fitness score at the initial iteration of evaluation. The property ω of dynamic nonlinear is applied to the degree of effect of the new position. The weighted update is formulated in Eq. 3.19 and Eq. 3.20,

$$\begin{cases} X(t+1) = \omega \cdot X_{\text{best}}\,(t) - A \cdot D_{\text{dist}} \\ D_{\text{dist}} \;= |C \cdot X_{\text{best}}\,(t) - X(t)| \end{cases} \tag{3.19}$$

$$\begin{cases} X(t+1) = O_{\text{dist}} \;\cdot \cos(2\pi l) \\ W = \omega \cdot X_{\text{best}}\,(t) \\ D_{\text{dist}} \;= |X_{\text{best}}\,(t) - X(t)| \end{cases} \tag{3.20}$$

The minimum adaptation scores ensure that it has highest inertia weight and maximum adaptation scores ensure it has a minimum inertia weight that is helpful for the performance of global optimum.

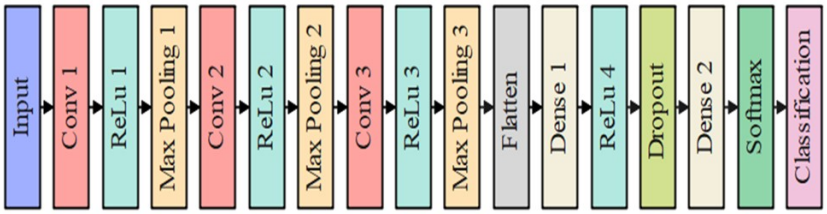

Fig. 3.3: Architecture of CNN

3.5.3. Differential Evolutionary Algorithm. The DEA includes three different processes such as variation, crossover and selection. Three controller parameters are there, such as differential variation parameter F, crossover probability CR and population size. Initially, the DE provides a new variance vector production measured by F. Then, crossover operation among target vector and variance is established, and the trial vector is produced. Atlast, the greedy selection is accomplished on target and trial vector then select an individuals with best fitness and come to next iteration procedure. After population initialization, three equally various vectors X_{r1}, X_{r2}, X_{r3} are randomly selected and a new variation vector is produced which is represented in Eq. 3.21,

$$V_i = X_{r1} + F \cdot (X_{r2} - X_{r3}) \tag{3.21}$$

where the F is a variance vector which is a random number within the range of $[0, 1]$. After mutation operation which produces a mutation vector, crossover is accomplished among target vector and variance to produce a test vector. The two crossover techniques are exponential and binomial crossover. Among them, binomial is utilized which is formulated in Eq. 3.22,

$$U'_{i,j} = \begin{cases} V_{i,j}, & \text{rand}_{i,j}[0,1] \leq CR \\ x_{i,j}, & \text{otherwise} \end{cases} \tag{3.22}$$

where $V_{i,j}$ is the i th individual of j th dimension produced in the above steps. $\text{rand}_{i,j}[0, 1]$ are the random number ranges of $[0, 1]$. The CR is a factor of crossover random number range of $[0, 1]$. After generating the test vectors, the fitness scores are related to the target vector. The individual with best fitness score is chosen for the next iteration. The f_{fit} is fitness function and the scientific equation of the selection operation is presented in Eq. 3.23,

$$X_i(t+1) = \begin{cases} U_i(t), & f_{\text{fit}}\ (X_i(t)) \\ X_i(t), & \text{Otherwise} \end{cases} \tag{3.23}$$

The selection process is separated into binary categories such as synchronous and asynchronous selection in which the asynchronous provides better performance than synchronous selection. In asynchronous, after recently produced test vector is associated with a target vector and best test vector instantly exchanges an equivalent target vector in a population. Hence, convergence speed of this algorithm is quicker.

3.6. Classification. The selected features are classified by using the Convolutional Neural Network (CNN) model which provides significant results in various areas such as image processing, Natural Language Processing (NLP) and diagnosis systems. The Multi-Layer Perceptron (MLP) and CNN decrease the number of parameters and neurons that results in quick adaptation with minimum complexity. The CNN has important applications in clinical image classification. The CNN is a kind of Feed-Forward Neural Network (FFNN) and DL model [25]. The convolution operation captures convention invariance that means the filter is independent in position that decreases a number of parameters. The CNN has three types of layers Convolution, pooling, and Fully Connected FC layers. Figure 3.3 represents CNN architecture.

These layers are essential for accomplishing dimensionality reduction, feature extractions and classifications. Through forward pass of a convolution operation, the filter is slid on computers and the input capacity of an activation map evaluates point-wise result of every score added and obtains the activation. The sliding filter is employed by linear and convolution operators, it is stated as a quick distribution of dot product. Consider w is the kernel function, x is the input, $(x \times w)(a)$ on time t is formulated as Eq. 3.24,

$$(x \times w)(a) = \int x(t)w(a-t)da \tag{3.24}$$

where a is R^n for each $n \geq 1$. The parameter t is the discrete which is presented in Eq. 3.25,

$$(x \times w)(a) = \sum_a x(t)w(t-a) \tag{3.25}$$

In this paper, the CNN is utilized for multi-classification problems. The 2D image I as input, K is a 2D kernel and convolution is formulated as Eq. 3.26,

$$(I \times K)(i,j) = \sum_m \sum_n I(m,n)K(i-m, j-n) \tag{3.26}$$

To improve the non-linearity, two different activation functions are utilized ReLU and softmax. The ReLU is represented as Eq. 3.27,

$$\text{ReLU}(x) = \max(0,x)x \in R \tag{3.27}$$

The gradient $\text{ReLU}(x) = 1$ for $x > 0$ and $\text{ReLU} -(x) = 0$ for $x < 0$. The ReLU convergence ability is better than the sigmoid non-linearities. The next layer is softmax, it is preferable when the result requires to include two or more classes which is mathematically formulated as Eq. 3.28,

$$\text{softmax}\,(x_i) = \frac{\exp\,(x_i)}{\sum_j \exp\,(x_i)} \tag{3.28}$$

The pooling layers are applied to result in a statistic of input and rescale the structure of output without missing essential data. There are various types of pooling layers, this paper utilized the highest pooling which individually produces large values in a rectangular neighbor of individual points (i,j) in 2D information for every input feature correspondingly. The FC is a last layer with m and n output and input are illustrated. The parameter of the output layer is stated as weight matrix $W \in M_{m,n}$. Where m and n an rows and columns and the bias vector $b \in R^m$. Consider as an input vector $x \in R^n$, the FC layer output through an activation function f is formulated as Eq. 3.29,

$$FC(x) := f(Wx = b) \in R^m \tag{3.29}$$

where Wx is the matrix product while function f is employed as a component. This fully connected layer is applied for classification difficulties. The FC layer of CNN is commonly involved at the topmost level. The CNN production is compressed and displayed as a single vector.

4. Experimental Result. In this paper, the proposed Whale Optimization Algorithm (WOA) based Convolutional Neural Network (CNN) model is stimulated by utilizing a python environment with the system configuration: RAM:16GB, processor: intel core i7 and operating system: windows 10. The parameters like accuracy, precision, sensitivity, specificity and F1-score are utilized to evaluate the model performance. The mathematical representation of these parameters is shown in Eq. 4.1, Eq. 4.2, Eq. 4.3, Eq. 4.4 and Eq. 4.5,

$$Accuracy = \frac{TP + TN}{TP + TN + FP + FN} \tag{4.1}$$

$$\text{Precision } = \frac{TP}{TP + FP} \tag{4.2}$$

Table 4.1: Memory usage

Image Size	RAM (GB)	
	With Feature Selection	Without Feature Selection
50	3.5	3.0
100	4.0	4.5
150	4.0	4.0
200	4.5	5.0
250	4.5	5.0
305	5.0	5.5

Table 4.2: Performance of Optimization Algorithm

Methods	Accuracy (%)	Precision (%)	Sensitivity (%)	Specificity (%)	F1-Score (%)
PSO	85.83	85.52	85.34	85.04	85.75
GJO	87.62	87.41	87.29	87.59	87.31
ABC	88.71	88.63	88.52	88.49	88.09
WOA	90.98	90.54	90.61	90.47	90.76
DECWOA	92.86	92.73	92.29	92.01	92.57

$$\text{Sensitivity} = \frac{TP}{TP + FN} \tag{4.3}$$

$$\text{Specificity} = \frac{TN}{TN + FP} \tag{4.4}$$

$$F1 - \text{score} = 2 \times \frac{\text{Precision} \times \text{sensitivity}}{\text{Precision} + \text{sensitivity}} \tag{4.5}$$

where TP, TN, FP and FN illustrate the True Positive, True Negative, False Positive and False Negatives respectively.

4.1. Quantitative Analysis. This section shows the quantitative analysis of the DECWOA model in terms of accuracy, precision, sensitivity, specificity and f1-score are shown in Table 4.1 4.2, 4.3 and 4.4. Table 4.1 illustrates the memory usage of various image size in terms of with and without feature selection. Table 4.2 illustrates the quantitative analysis of various optimizations by employing chest X-ray images dataset. Table 4.3 illustrates the quantitative analysis of various classifiers with default features. Table 4.4 illustrates the quantitative analysis of various classifiers after feature selection.

Table 4.2 and Figure 4.1 represent the performance of the optimization algorithm by using performance metrics like accuracy, precision, sensitivity, specificity and f1-score. The performance of Particle Swarm Optimization (PSO), Golden Jackal Optimization (GJO), Artificial Bee Colony (ABC) and Whale Optimization Algorithm (WOA) are compared with DECWOA. The attained result displays that the DECWOA attains an accuracy of 92.86%, precision of 92.73%, sensitivity of 92.29%, specificity of 92.01%, and f1-score of 92.57% which is comparatively higher than the existing optimization algorithms.

Table 4.3 and Figure 4.2 represents the performance of classification with default features by using performance metrics like accuracy, precision, sensitivity, specificity and f1-score. The performance of Artificial Neural Network (ANN), K-Nearest Neighbour (KNN), Support Vector Machine (SVM) and Deep Neural Network (DNN) are compared with CNN model. The attained result displays that the CNN model attains accuracy of 93.97%, precision of 93.57%, sensitivity of 93.71%, specificity of 93.49% and f1-score of 93.85% which is higher than the existing classifiers.

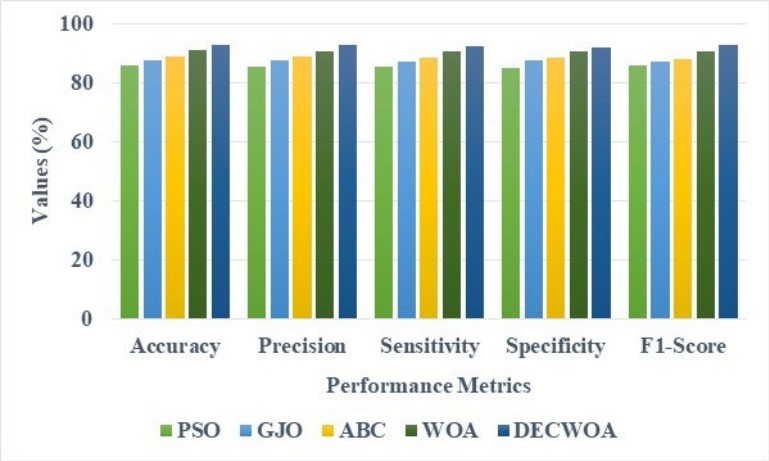

Fig. 4.1: Performance of Optimization Algorithm

Table 4.3: Performance of classification with default features

Methods	Accuracy (%)	Precision (%)	Sensitivity (%)	Specificity (%)	F1-Score (%)
ANN	84.53	84.21	84.01	84.33	84.49
KNN	87.91	87.02	87.63	87.47	87.89
SVM	89.76	89.24	89.54	89.21	89.72
DNN	91.63	91.27	90.49	91.03	91.43
CNN	93.97	93.57	93.71	93.49	93.85

Table 4.4 and Figure 4.3 represent the performance of classification after feature selection by using evaluation metrics like accuracy, precision, sensitivity, specificity, and f1-score. The performance of ANN, KNN, SVM and DNN are compared with DECWOA-CNN model. The attained result displays that the DECWOA-CNN model attains accuracy of 99.89%, precision of 99.83%, sensitivity of 99.81%, specificity of 98.92% and f1-score of 99.26% which is comparatively higher than the existing methods.

4.2. Comparative Analysis. This section illustrates the comparative analysis of the proposed DECWOA-CNN model with performance metrics like accuracy, precision, sensitivity, specificity and f1-score as shown in Table 4.5. The existing result such as [15] [16], [17], [18] and [20] are utilized for estimating an ability of the classifier. The DECWOA-CNN is trained, tested and validated by using CXR dataset. The result obtained from Table 4.5 shows that the DECWOA-CNN attains better performance when compared with the existing methods. The accuracy was improved to 99.89%, precision of 99.83%, sensitivity of 99.81%, specificity of 98.92% and f1-score of 99.26%.

4.2.1. Discussion. In this section, the advantages of the proposed method and the limitations of existing methods are discussed. The existing method has some limitations such as the ET-NET [15] was incapable of detecting the current COVID-19 infections from the initial infection stage. The ResNet50 [16] model carrying out transfer learning on the limited clinical image dataset and computing resources. The VGG-19 [17] model employed MongoDB for storing images, once it crossed 16MB size then it cannot be retained. The MMF-DTL [18] model cannot be tested on real-time images. The VGG19-RNN [20] has works only with anterior-posterior view in chest X-ray so, it is unable to classify other views like lordotic, apical. The proposed DECWOA-CNN model overcomes these existing model limitations. The proposed model improves the accuracy and convergence speed of the optimization algorithm.

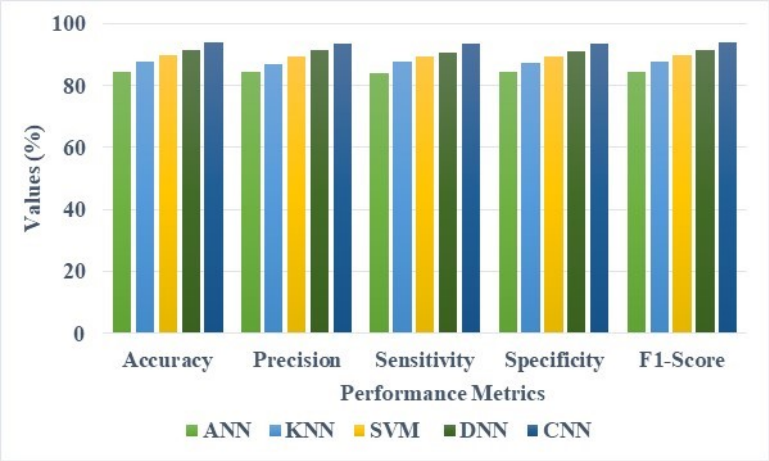

Fig. 4.2: Performance of classification with default features

Table 4.4: Performance of classification after feature selection

Methods	Accuracy (%)	Precision (%)	Sensitivity (%)	Specificity (%)	F1- Score (%)
ANN	84.53	84.21	84.01	84.33	84.49
KNN	87.91	87.02	87.63	87.47	87.89
SVM	89.76	89.24	89.54	89.21	89.72
DNN	91.63	91.27	90.49	91.03	91.43
DECWOA-CNN	99.89	99.83	99.81	98.92	99.26

5. Conclusion. This paper proposed a DECWOA-CNN model for accurately and quickly identifying and classifying COVID-19. The median filter is utilized for data pre-processing which removes the noise from chest X-ray images and fed into threshold segmentation for segmenting chest-ray images. The shape, texture, color and ResNet-50 feature extraction is utilized for extracting features from segmented images. The DECWOA is utilized for selecting features and CNN is utilized for classifying COVID-19 from chest images. In DECWOA, initial population is produced by presenting the Sine Chaos theory at the start of an algorithm for improving popularity diversity. Then, the new adaptive inertia weight is familiarized into whale individual position update formulation to untrained global search and enhancing optimization performance. At last, DEA is presented to enhance whale optimization accuracy and global search speed. The proposed DECWOA-CNN model is estimated on CXR dataset and attains better results by using performance metrics like accuracy, precision, sensitivity, specificity, and F1-score values of about 99.89%, 99.83%, 99.81%, 98.92%, and 99.26% respectively. In the future, the parameter tuning will be applied in the optimization algorithm to improve the model performance.

REFERENCES

[1] M. M. Taresh, N. Zhu, T. A. A. Ali, A. S. Hameed, and M. L. Mutar, *Transfer learning to detect covid-19 automatically from x-ray images using convolutional neural networks*, Int. J. Biomed. Imaging, (2021), pp. 1–9.

[2] E. Jangam, A. A. D. Barreto, and C. S. R. Annavarapu, *Automatic detection of COVID-19 from chest CT scan and chest X-Rays images using deep learning, transfer learning and stacking*, Appl. Intell., (2022), pp.1–17.

[3] Y. Brima, M. Atemkeng, S. Tankio Djiokap, J. Ebiele, and F. Tchakounté, *Transfer learning for the detection and diagnosis of types of pneumonia including pneumonia induced by COVID-19 from chest X-ray images*, Diagnostics, 11(8) (2021), p. 1480.

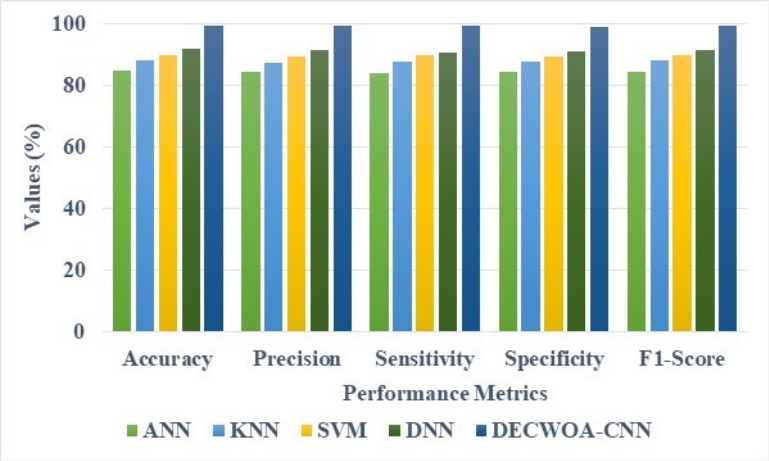

Fig. 4.3: Performance of classification after feature selection

Table 4.5: Comparative Analysis

Author	Dataset	Accuracy (%)	Precision (%)	Sensitivity (%)	Specificity (%)	F1-Score (%)
Rohit Kundu et al. [15]	CXR	97.81	97.77	97.81	N/A	97.77
Md. Belal Hossain et al. [16]		99.17	99.31	99.03	N/A	99.17
Soarov Chakraborty et al. [17]		97.11	97	97	N/A	97
A. Siva Krishna Reddy et al. [18]		98.80	93.60	92.96	98.54	93.26
Md. Milon Islam et al. [20]		99.86	99.78	99.78	N/A	99.78
Proposed DECWOA-CNN Model		99.89	99.83	99.81	98.92	99.26

[4] S. Showkat and S. Qureshi, *Efficacy of Transfer Learning-based ResNet models in Chest X-ray image classification for detecting COVID-19 Pneumonia*, Chemometrics and Intelligent Laboratory Systems, 224 (2022), p. 104534.
[5] S. Amin, B. Alouffi, M. I. Uddin, and W. Alosaimi, *Optimizing convolutional neural networks with transfer learning for making classification report in covid-19 chest x-rays scans*, Sci. Program., 2022 (2022).
[6] M. Umair, M. S. Khan, F. Ahmed, F. Baothman, F. Alqahtani, M. Alian, and J. Ahmad, *Detection of COVID-19 using transfer learning and grad-cam visualization on indigenously collected X-ray dataset*, Sensors, 21(17) (2021), p. 5813.
[7] M. T. Naseem, T. Hussain, C. S. Lee, and M. A. Khan, *Classification and Detection of COVID-19 and Other Chest-Related Diseases Using Transfer Learning*, Sensors, 22(20) (2022), p. 7977.
[8] G. Li, R. Togo, T. Ogawa, and M. Haseyama, *COVID-19 detection based on self-supervised transfer learning using chest X-ray images*, Int. J. Comput. Assisted Radiol. Surg., 18(4) (2023), pp. 715–722.
[9] S. Hamida, O. El Gannour, B. Cherradi, A. Raihani, H. Moujahid, and H. Ouajji, *A novel COVID-19 diagnosis support system using the stacking approach and transfer learning technique on chest X-ray images*, J. Healthcare Eng., 2021 (2021).
[10] W. A. Hamwi and M. M. Almustafa, *Development and integration of VGG and dense transfer-learning systems supported with diverse lung images for discovery of the Coronavirus identity*, Inf. Med. Unlocked, 32 (2022), p. 101004.
[11] S. Asif, Y. Wenhui, K. Amjad, H. Jin, Y. Tao, and S. Jinhai, *Detection of COVID-19 from chest X-ray images: Boosting the performance with convolutional neural network and transfer learning*, Expert Syst., 40(1) (2023), p. e13099.
[12] J. Manokaran, F. Zabihollahy, A. Hamilton-Wright, and E. Ukwatta, *Detection of COVID-19 from chest x-ray images using transfer learning*, J. Med. Imaging, 8(S1) (2021), pp. 017503–017503.

[13] S. Agrawal, V. Honnakasturi, M. Nara, and N. Patil, *Utilizing Deep Learning Models and Transfer Learning for COVID-19 Detection from X-Ray Images*, SN Comput. Sci., 4(4) (2023), p. 326.
[14] A. U. Haq, J. P. Li, S. Ahmad, S. Khan, M. A. Alshara, and R. M. Alotaibi, *Diagnostic approach for accurate diagnosis of COVID-19 employing deep learning and transfer learning techniques through chest X-ray images clinical data in E-healthcare*, Sensors, 21(24) (2021), p. 8219.
[15] R. Kundu, P. K. Singh, M. Ferrara, A. Ahmadian, and R. Sarkar, *ET-NET: an ensemble of transfer learning models for prediction of COVID-19 infection through chest CT-scan images*, Multimedia Tools Appl., 81(1) (2022), pp. 31–50.
[16] M. B. Hossain, S. H. S. Iqbal, M. M. Islam, M. N. Akhtar, and I. H. Sarker, *Transfer learning with fine-tuned deep CNN ResNet50 model for classifying COVID-19 from chest X-ray images*, Inf. Med. Unlocked, 30 (2022), p. 100916.
[17] S. Chakraborty, S. Paul, and K. A. Hasan, *A transfer learning-based approach with deep cnn for covid-19-and pneumonia-affected chest x-ray image classification*, SN Comput. Sci., 3 (2022), pp. 1–10.
[18] A. S. K. Reddy, K. B. Rao, N. R. Soora, K. Shailaja, N. S. Kumar, A. Sridharan, and J. Uthayakumar, *Multi-modal fusion of deep transfer learning based COVID-19 diagnosis and classification using chest x-ray images*, Multimedia Tools Appl., 82(8) (2023), pp. 12653–12677.
[19] P. L. Vidal, J. de Moura, J. Novo, and M. Ortega, *Multi-stage transfer learning for lung segmentation using portable X-ray devices for patients with COVID-19*, Expert Syst. Appl., 173 (2021), p. 114677.
[20] M. M. Islam, M. Z. Islam, A. Asraf, M. S. Al-Rakhami, W. Ding, and A. H. Sodhro, *Diagnosis of COVID-19 from X-rays using combined CNN-RNN architecture with transfer learning*, BenchCouncil Trans. Benchmarks Stand. Eval., 2(4) (2022), p. 100088.
[21] N. Kumar, M. Gupta, D. Gupta, and S. Tiwari, *Novel deep transfer learning model for COVID-19 patient detection using X-ray chest images*, J. Ambient Intell. Hum. Comput., 14(1) (2023), pp. 469–478.
[22] Dataset Link : https://www.kaggle.com/datasets/alifrahman/chestxraydataset.
[23] A. Sharma and P. K. Mishra , Image enhancement techniques on deep learning approaches for automated diagnosis of COVID-19 features using CXR images, Multimedia Tools Appl., 81(29) (2022), pp. 42649–42690.
[24] J. Xing, H. Zhao, H. Chen, R. Deng, and L. Xiao, *Boosting whale optimizer with quasi-oppositional learning and gaussian barebone for feature selection and COVID-19 image segmentation*, J. Bionic Eng., 20(2) (2023), pp. 797–818.
[25] D. Zhang, F. Ren, Y. Li, L. Na, and Y. Ma, *Pneumonia detection from chest X-ray images based on convolutional neural network*, Electronics, 10(13) (2021), p. 1512.

Edited by: Chiranji Lal Chowdhary
Special issue on: Scalable Machine Learning for Health Care: Innovations and Applications
Received: Oct 13, 2023
Accepted: Dec 20, 2023